Nanoscale

COMMUNICATION

View Article Online
View Journal | View Issue

Cite this: *Nanoscale*, 2017, **9**, 11434

Received 11th June 2017,
Accepted 28th July 2017

DOI: 10.1039/c7nr04161f

rsc.li/nanoscale

Visible-light driven Si–Au micromotors in water and organic solvents†

Dekai Zhou,‡[a,b] Yuguang C. Li,‡[b] Pengtao Xu,[b] Liqiang Ren,[b] Guangyu Zhang,[a] Thomas E. Mallouk*[b] and Longqiu Li*[a]

We report the fabrication of tadpole-shaped Si–Au micromotors using glancing angle deposition. These micromotors are activated by visible light and can move in either deionized water or organic solvents without the addition of chemical fuels. By controlling the light intensity, the velocity of the micromotors can be modulated and the motion can be switched on and off reversibly. Gas chromatographic measurements and buffered oxide etch (BOE) experiments show that the mechanism of propulsion is self-electrophoresis modulated by the photoconductivity of the amorphous silicon segment. The direction of motion of the microswimmers can also be controlled by applying an external magnetic field if a ferromagnetic Ni layer is added in the fabrication process.

Nano/micromotors are nano/microscale devices that can locally convert environmental energy into mechanical energy.[1–3] Since the first catalytic nanomotors were proposed by Paxton *et al.* in 2004,[4] many different types of energy sources including chemical,[4–7] magnetic,[8–13] electrical,[14–16] acoustic,[17–21] light[22–29] and thermal[30,31] have been employed to power nano/micromotors. The corresponding propulsion mechanisms for these nano/micromotors have also been determined.[4,20,30,32–34] Compared to other types of energy input for microswimmer propulsion, light energy is biocompatible, highly efficient, and easily switched on and off. Two basic principles of light energy conversion for nano/micromotors have been demonstrated, namely, photothermal[30,35–38] and photoelectric effects.[22,24,25,39] In the case of photothermal nano/micromotors, near infrared illumination leads to a thermal gradient that propels the particles, and gold nanoparticles are commonly employed. For those propelled by the photoelectric effect, semiconductor materials in which electron–hole pairs are generated are commonly employed. The photochemically generated electrons and holes drive chemical reactions, *e.g.* hydrogen peroxide decomposition, resulting in self-propulsion.[23–26,39,40] For light-powered nano/micromotors, the wavelength of light and the tolerance of different chemical environments are two key challenges for analytical, biomedical and environmental applications. Most of the light-driven motors reported to date require either ultraviolet (UV) light[24,25] or added toxic chemicals (such as hydrogen peroxide or aqueous halogens)[22] as fuels and thus are not appropriate for applications in living cells or for *in vivo* applications such as drug delivery. Recently, several studies have been carried out by our group[27] and by Dong *et al.*[29] with the goal of expanding the light wavelength to the visible and tissue-transparent near-infrared region of the spectrum. Narrow band gap semiconductor materials including Cu_2O[27] and BiOI[27,29] have been used. These visible-light-driven nano/micromotors have been studied in low concentrations of aqueous hydrogen peroxide solutions and in deionized (DI) water. In addition to aqueous solutions, organic solvents are also widely used and are important in environmental cleaning and in biomedical diagnostics.[41,42] In addition, the two aforementioned visible-light-driven nano/micromotors are Janus microspheres. Thus, in order to expand the utility of synthetic micromotors, it is important to develop microrod-based nano/micromotors that can absorb visible and near-infrared light for propulsion in various media.

In order to absorb light at longer wavelengths, narrow band gap semiconductor materials are needed. Silicon is the most widely used semiconductor in solar cells, integrated circuits and semiconductor devices,[43,44] and it absorbs both visible and near-infrared light. In addition, the conduction band of silicon is sufficiently negative to decompose water or protic organic solvents into hydrogen. Esplandiu *et al.*[45] recently reported a micropump consisting of Pt patches on a silicon substrate, in which electro-osmotic flow is driven photochemically. In order to make autonomous micromotors that operate on the same principle, we synthesized Si–Au microrods using

[a]*Key Laboratory of Microsystems and Microstructures Manufacturing, Harbin Institute of Technology, Harbin, Heilongjiang 150001, P.R. China. E-mail: longqiuli@hit.edu.cn*

[b]*Departments of Chemistry, Biochemistry and Molecular Biology, and Physics, The Pennsylvania State University, University Park, PA 16802, USA. E-mail: tem5@psu.edu*

†Electronic supplementary information (ESI) available. See DOI: 10.1039/c7nr04161f

‡These authors contributed equally to this work.

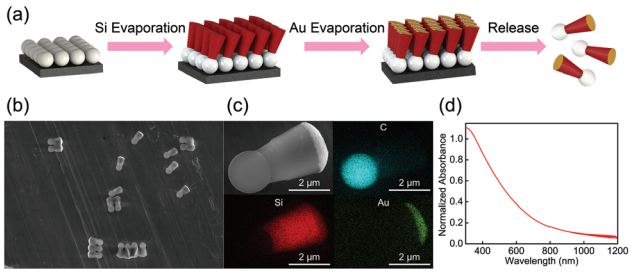

Fig. 1 Fabrication and characterization of Si–Au microparticles: (a) schematic of the GAD fabrication process. (b) SEM image. (c) EDS images showing the C, Au and Si elemental distribution on a Si–Au micromotor. (d) UV-Vis absorbance spectrum of a 10 nm thick Si film on a glass slide.

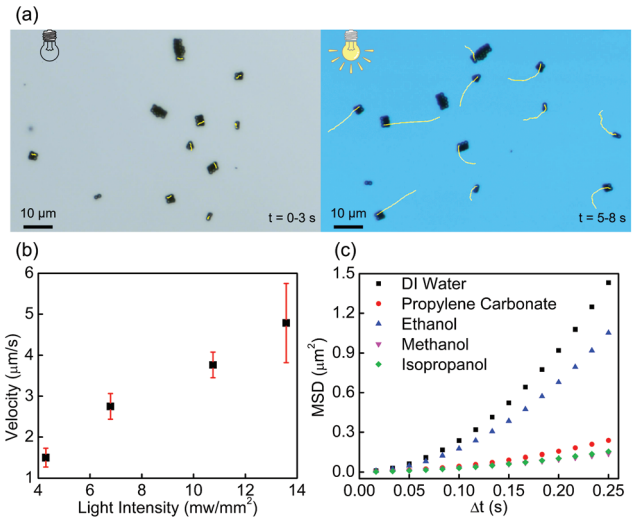

Fig. 2 (a) Trajectories of the Si–Au micromotors in water, from left to right, without illumination (Δt = 3 s), and with illumination (Δt = 3 s) at a light intensity of 13.6 mW mm^{-2}. (b) Speeds of the Si–Au micromotors under different light intensities in DI water. (c) Speeds of the Si–Au micromotors in different solvents, illuminated at 13.6 mW mm^{-2}.

glancing angle deposition. We report here visible light-driven microscale Si–Au motors that display autonomous motion both in DI water and organic solvents without the addition of chemical fuels. By controlling the light intensity, the velocity of the Si–Au micromotors can be tuned and the motion can be quickly started and stopped by switching the light on and off.

Si nano/microstructures can be synthesized by a number of methods including lithography, chemical vapor deposition and template-growth methods.[46–50] However, some of these methods offer poor control of particle size,[47] and others require expensive instrumentation or complicated fabrication procedures.[46,48,49] Glancing angle deposition (GAD) is a relatively simple technique that enables complex microstructures to be fabricated. By controlling the parameters of deposition, *e.g.* the deposition angle, power and time, the size and shape of the micromotors can be easily modified, and multilayered structures can be realized from different materials. The fabrication of Si–Au microrods by GAD is shown schematically in Fig. 1(a).[51–53] Polystyrene microspheres were first drop-cast onto a Si wafer and dried to form a monolayer. Then a 3 μm thick layer of Si was deposited onto the polystyrene microspheres at an angle of 5° from the surface normal. Due to the close packing of the polystyrene microspheres, tapered Si microrods were obtained. Au was then evaporated onto the Si rods. Finally, the micromotors were released in DI water or organic solvents by sonication (see the Materials and methods section in the ESI†). Fig. 1(b) shows a scanning electron microscope (SEM) image of the Si–Au micromotors, which have a conical shape with a length of approximately 5 μm. Energy dispersive X-ray spectroscopy (EDS) mapping shown in Fig. 1(c) indicates that the polystyrene–Si–Au micromotors contain only C, Si, and Au, as expected. Fig. 1(d) shows the UV-visible absorbance spectrum of a 10 nm thick Si film on a glass substrate. As can be seen from the figure, the Si (which is amorphous according to X-ray diffraction data as shown in Fig. S-1†) begins to absorb in the near-infrared at wavelengths shorter than 1000 nm and is strongly absorbing throughout the visible part of the spectrum.

When the Si–Au micromotors were suspended in DI water, they exhibited slow, random movement as shown in Fig. 2(a). However, when they were illuminated by a mercury lamp with a 380 nm cut-off filter, fast and autonomous motion was observed (Fig. 2(a) and Video S-1†). The Si–Au micromotors move with the Si end leading at a speed of up to 5 μm s^{-1} at a light intensity of 13.6 mW mm^{-2}. After illumination for about 10 min, the axial propulsion of the motors was no longer observable and they underwent random motion only. In order to understand the visible light propulsion behaviour, the relative contributions of two factors were investigated: the light intensity and the composition of the electrolyte solution. We varied the light intensity from 13.6 mW mm^{-2} to 4.3 mW mm^{-2} using neutral density filters and observed that the initial speed was proportional to the light intensity, suggesting a light-limited propulsion mechanism (Fig. 2(b)). In addition, we measured the velocity of Si–Au micromotors in different solvents. We observed that the micromotors can move in DI water, ethanol, methanol, isopropanol, and propylene carbonate (Fig. 2c and Video S-2†). Based on these results, we conclude that the light intensity and electrolyte solution both affect the speed of the Si–Au micromotors. It was also clear that the micromotors move in DI water and in polar organic solvents without added fuels such as hydrogen peroxide or halogens.

In order to understand the propulsion mechanism of the Si–Au micromotors, several experiments were performed. First, the micromotors were dispersed in DI water and irradiated by visible light for 50 min. After that, the motion of the micromotors at a light intensity of 13.6 mW mm^{-2} was evaluated under a microscope. Si–Au micromotors that had been exposed to light for 50 min showed only Brownian motion (Fig. 3(a) and Video S-3†). This experiment seems to rule out a photothermophoretic mechanism, since the Si–Au micromotors were not visibly changed and still absorbed light. Alternatively, it is

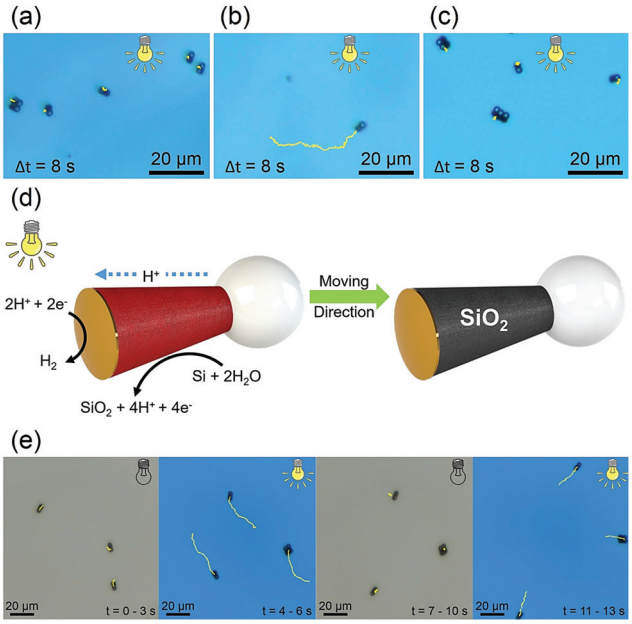

Fig. 3 (a) The trajectories of the Si–Au micromotors in DI water after irradiation with a 100 mW cm^{-2} visible light for 50 minutes and observed at a light intensity of 13.6 mW mm^{-2} on an optical microscope(Δt = 8 s). (b) Trajectories after etching in 10% BOE solution; light intensity was 13.6 mW mm^{-2} (Δt = 8 s). (c) Trajectories in DI water with 0.5 mM $NaNO_3$; light intensity was 13.6 mW mm^{-2} (Δt = 8 s). (d) Propulsion mechanism of the Si–Au micromotors activated by visible light in DI water. (e) Time-lapse snapshots showing trajectories of Si–Au micromotors in DI water during light switching.

possible that the surface of Si was oxidized to SiO_2 after prolonged irradiation and this blocked the propulsion by creating an insulating surface layer. In order to test this hypothesis, another experiment was conducted in which light-treated Si–Au micromotors were collected and etched with 10% buffered oxide etch (BOE) solution for one minute, a procedure that is used to etch the native oxide layer from silicon wafers.[54,55] After etching, the micromotors were washed with DI water several times and re-suspended in DI water. We observed, as shown in Fig. 3(b), that this treatment restored the powered movement under visible light illumination (Video S-3†). Based on these results, we conclude that the Si surface is oxidized into SiO_2 under illumination. In order to balance this oxidation reaction, a reduction reaction must also occur. We postulated that water was reduced to hydrogen in a bipolar electrochemical reaction. This hypothesis was supported by the detection of hydrogen by gas chromatography (GC) from micromotors irradiated by visible light for 1 h in water. No hydrogen was detected in the absence of Si–Au micromotors or without illumination. The simultaneous occurrence of oxidation and reduction at the surface of the micromotors suggests a light-driven bipolar electrophoretic mechanism for propulsion. The reactions on the two ends are depicted in Fig. 3(d): at the Si end, Si is oxidized to SiO_2, and protons are generated. Protons are consumed on the Au side in the catalytic reaction that produces hydrogen. The resulting proton gradient results in an electric field that exerts a force on the particles, which typically have a negative surface charge at neutral pH, propelling them towards the Si end. The catalytic reactions under visible light are given by eqn (1) and (2):

On the Si side:

$$Si + 2H_2O \rightarrow SiO_2 + 4H^+ + 4e^- \quad (1)$$

On the Au side:

$$4H^+ + 4e^- \rightarrow 2H_2 \quad (2)$$

It is also important to note that the amorphous Si segment of the motors is likely to be insulating in the dark and photoconductive. Amorphous Si typically has a mobility gap of about 1.7 eV and is photoconductive in visible light. Thus, when the micromotors are irradiated with visible light, the bipolar electrochemical reaction accelerates the surface oxidation of Si and the reduction of water at the Au surface. The propulsion mechanism in organic solvents is similar to that in DI water, presumably because of the presence of trace water that can support the bipolar electrochemical reaction. It should be noted from Fig. 2(c) that the speed in organic solvents is significantly slower than in water. This can be attributed to the slow kinetics of the anode and cathode reactions in organic solvents, and also to the lower activity of protons. For electrophoretically driven nano/micromotors, the velocity is expected to decrease in salt solutions – a definitive method for differentiating self-electrophoresis from thermophoresis and other propulsion mechanisms.[56,57] The Si–Au micromotors exhibited only Brownian motion when illuminated in DI water in the presence of 0.5 mM $NaNO_3$ as shown in Fig. 3(c) and Video S-3,† which supports the proposed electrophoretic propulsion mechanism.

The Si–Au micromotors show excellent external controllability. This was demonstrated by rapid start/stop motion using light switching (Video S-4†). Fig. 3(e) illustrates that the micromotors exhibit only slow random motion in the absence of light, but immediately start to move when the light is switched on. This kind of fast response and on/off switching can be useful in a range of applications, as well as in fundamental studies of phototaxis and collective phenomena. In addition, the ability to steer the micromotors is useful. By sputtering a 10 nm thick Ni layer on the polystyrene microparticles, as illustrated in Fig. S-2(a),† the Si–Au micromotors were steered by an external magnetic field, as shown in Fig. S-2(b) and Video S-5.†

In conclusion, Si–Au micromotors were synthesized by glancing angle deposition. Due to the narrow bandgap and relatively negative conduction band edge potential of Si, the micromotors can be activated by visible light, reducing water to hydrogen and oxidizing the Si surface to SiO_2. Their speed is modulated by changing the light intensity. GC measurements and BOE experiments supported a light-induced self-electrophoretic propulsion mechanism. Additionally, the movement could be steered by an external magnetic field with an additional Ni layer on the polystyrene microparticles. The key

characteristics of these visible light induced micromotors are their fuel-free motion in both DI water and organic solvents. The use of a narrow-gap semiconductor thus extends the useful wavelength range and solvent environments for micromotors.

Acknowledgements

This work was supported by the National Science Foundation under MRSEC grant number DMR-1420620. D. Zhou, G. Zhang and L. Li are grateful for the financial support from the National Natural Science Foundation of China (51521003 and 51175129), Key Laboratory of Micro-systems and Micro-structures Manufacturing of Ministry of Education (2016KM004), Program of Introducing Talents of Discipline to Universities (Grant No. B07018) and Self-Planned Task of State Key Laboratory of Robotics and System (HIT) (SKLRS 201706A).

Notes and references

1 T. E. Mallouk and A. Sen, *Sci. Am.*, 2009, **300**, 72–77.
2 J. Wang, *ACS Nano*, 2009, **3**, 4–9.
3 K. Kim, J. Guo, Z. X. Liang, F. Q. Zhu and D. L. Fan, *Nanoscale*, 2016, **8**, 10471.
4 W. F. Paxton, K. C. Kistler, C. C. Olmeda, A. Sen, S. K. St Angelo, Y. Cao, T. E. Mallouk, P. E. Lammert and V. H. Crespi, *J. Am. Chem. Soc.*, 2004, **126**, 13424–13431.
5 S. Fournier-Bidoz, A. C. Arsenault, I. Manners and G. A. Ozin, *Chem. Commun.*, 2005, 441–443, DOI: 10.1039/B414896G.
6 M. Pumera, *Nanoscale*, 2010, **2**, 1643–1649.
7 L. Li, J. Wang, T. Li, W. Song and G. Zhang, *Soft Matter*, 2014, **10**, 7511.
8 S. Tottori, L. Zhang, F. Qiu, K. K. Krawczyk, A. Franco-Obregón and B. J. Nelson, *Adv. Mater.*, 2012, **24**, 811–816.
9 P. Fischer and A. Ghosh, *Nanoscale*, 2011, **3**, 557–563.
10 A. Ghosh and P. Fischer, *Nano Lett.*, 2009, **9**, 2243–2245.
11 T. Li, J. Li, H. Zhang, X. Chang, W. Song, Y. Hu, G. Shao, E. Sandraz, G. Zhang, L. Li and J. Wang, *Small*, 2016, **12**, 6098–6105.
12 A. Cebers and K. Erglis, *Adv. Funct. Mater.*, 2016, **26**, 3783–3795.
13 K. I. Morozov and A. M. Leshansky, *Nanoscale*, 2014, **6**, 1580.
14 P. Calvo-Marzal, S. Sattayasamitsathit, S. Balasubramanian, J. R. Windmiller, C. Dao and J. Wang, *Chem. Commun.*, 2010, **46**, 1623–1624.
15 S. T. Chang, V. N. Paunov, D. N. Petsev and O. D. Velev, *Nat. Mater.*, 2007, **6**, 235–240.
16 X. Xu, C. Liu, K. Kim and D. L. Fan, *Adv. Funct. Mater.*, 2014, **24**, 4843–4850.
17 D. Kagan, M. J. Benchimol, J. C. Claussen, E. Chuluun-Erdene, S. Esener and J. Wang, *Angew. Chem., Int. Ed.*, 2012, **51**, 7519–7522.
18 S. Ahmed, D. T. Gentekos, C. A. Fink and T. E. Mallouk, *ACS Nano*, 2014, **8**, 11053–11060.
19 S. Ahmed, W. Wang, L. O. Mair, R. D. Fraleigh, S. Li, L. A. Castro, M. Hoyos, T. J. Huang and T. E. Mallouk, *Langmuir*, 2013, **29**, 16113–16118.
20 W. Wang, L. A. Castro, M. Hoyos and T. E. Mallouk, *ACS Nano*, 2012, **6**, 6122–6132.
21 Z. Wu, T. Li, W. Gao, T. Xu, B. Jurado-Sánchez, J. Li, W. Gao, Q. He, L. Zhang and J. Wang, *Adv. Funct. Mater.*, 2015, **25**, 3881–3887.
22 M. Ibele, T. E. Mallouk and A. Sen, *Angew. Chem., Int. Ed.*, 2009, **48**, 3308–3312.
23 J. Palacci, S. Sacanna, A. P. Steinberg, D. J. Pine and P. M. Chaikin, *Science*, 2013, **339**, 936–940.
24 R. Dong, Q. Zhang, W. Gao, A. Pei and B. Ren, *ACS Nano*, 2016, **10**, 839–844.
25 C. Chen, F. Mou, L. Xu, S. Wang, J. Guan, Z. Feng, Q. Wang, L. Kong, W. Li, J. Wang and Q. Zhang, *Adv. Mater.*, 2017, **29**, 1603374.
26 Y. Hong, M. Diaz, U. M. Córdova-Figueroa and A. Sen, *Adv. Funct. Mater.*, 2010, **20**, 1568–1576.
27 D. Zhou, Y. C. Li, P. Xu, N. S. McCool, L. Li, W. Wang and T. E. Mallouk, *Nanoscale*, 2017, **9**, 75–78.
28 X. Xu, H. Li, H. Dihan, R. S. Ruoff, A. X. Wang and D. L. Fan, *Adv. Funct. Mater.*, 2013, **23**, 4273–4273.
29 R. Dong, Y. Hu, Y. Wu, W. Gao, B. Ren, Q. Wang and Y. Cai, *J. Am. Chem. Soc.*, 2017, **139**, 1722–1725.
30 H.-R. Jiang, N. Yoshinaga and M. Sano, *Phys. Rev. Lett.*, 2010, **105**, 268302.
31 L. Baraban, R. Streubel, D. Makarov, L. Han, D. Karnaushenko, O. G. Schmidt and G. Cuniberti, *ACS Nano*, 2013, **7**, 1360–1367.
32 R. A. Pavlick, S. Sengupta, T. McFadden, H. Zhang and A. Sen, *Angew. Chem., Int. Ed.*, 2011, **50**, 9374–9377.
33 H. Wang and M. Pumera, *Nanoscale*, 2017, **9**, 2109–2116.
34 Y. Mei, G. Huang, A. A. Solovev, E. B. Ureña, I. Mönch, F. Ding, T. Reindl, R. K. Y. Fu, P. K. Chu and O. G. Schmidt, *Adv. Mater.*, 2008, **20**, 4085–4090.
35 Y. Wu, T. Si, J. Shao, Z. Wu and Q. He, *Nano Res.*, 2016, **9**, 3747–3756.
36 Z. Wu, T. Si, W. Gao, X. Lin, J. Wang and Q. He, *Small*, 2016, **12**, 577–582.
37 Z. Wu, X. Lin, Y. Wu, T. Si, J. Sun and Q. He, *ACS Nano*, 2014, **8**, 6097–6105.
38 M. Xuan, Z. Wu, J. Shao, L. Dai, T. Si and Q. He, *J. Am. Chem. Soc.*, 2016, **138**, 6492–6497.
39 B. Dai, J. Wang, Z. Xiong, X. Zhan, W. Dai, C.-C. Li, S.-P. Feng and J. Tang, *Nat. Nanotechnol.*, 2016, **11**, 1087–1092.
40 M. Enachi, M. Guix, V. Postolache, V. Ciobanu, V. M. Fomin, O. G. Schmidt and I. Tiginyanu, *Small*, 2016, **12**, 5497–5505.
41 M. Priske, M. Lazar, C. Schnitzer and G. Baumgarten, *Chem. Ing. Tech.*, 2016, **88**, 39–49.
42 A. Bose and H. Keharia, *Biocatal. Agric. Biotechnol.*, 2013, **2**, 255–266.
43 M. G. Voronkov, *Russ. J. Appl. Chem.*, 2007, **80**, 2190–2196.
44 M. E. Weeks, *J. Chem. Educ.*, 1932, **9**, 1386.

45 M. J. Esplandiu, A. Afshar Farniya and A. Bachtold, *ACS Nano*, 2015, **9**, 11234–11240.
46 A. T. Heitsch, C. M. Hessel, V. A. Akhavan and B. A. Korgel, *Nano Lett.*, 2009, **9**, 3042.
47 Y. Li, M. Li, P. Fu, R. Li, D. Song, C. Shen and Y. Zhao, *Sci. Rep.*, 2015, **5**, 11532.
48 H. Lin, H. Y. Cheung, F. Xiu, F. Wang, S. P. Yip, N. Han, T. F. Hung, J. Zhou, J. C. Ho and C. Y. Wong, *J. Mater. Chem. A*, 2013, **1**, 9942–9946.
49 B. Ai, H. Möhwald, D. Wang and G. Zhang, *Adv. Mater. Interfaces*, 2016, **4**, 1600271.
50 L. Dupré, T. Gorisse, A. L. Lebranchu, T. Bernardin, P. Gentile, H. Renevier and D. Buttard, *Nanoscale Res. Lett.*, 2013, **8**, 123.
51 J. G. Gibbs and Y. Zhao, *Small*, 2010, **6**, 1656.
52 H. K. Raut, V. A. Ganesh, A. S. Nair and S. Ramakrishna, *Energy Environ. Sci.*, 2011, **4**, 3779–3804.
53 C. Wongchoosuk, A. Wisitsoraat, D. Phokharatkul, M. Horprathum, A. Tuantranont and T. Kerdcharoen, *Sens. Actuators, B*, 2013, **181**, 388–394.
54 H.-D. Um, N. Kim, K. Lee, I. Hwang, J. Hoon Seo, Y. J. Yu, P. Duane, M. Wober and K. Seo, *Sci. Rep.*, 2015, **5**, 11277.
55 W. Xia, J. Zhu, H. Wang and X. Zeng, *CrystEngComm*, 2014, **16**, 4289–4297.
56 S. Ebbens, D. A. Gregory, G. Dunderdale, J. R. Howse, Y. Ibrahim, T. B. Liverpool and R. Golestanian, *EPL*, 2014, **106**, 58003.
57 A. Brown and W. Poon, *Soft Matter*, 2014, **10**, 4016–4027.